

## AIAA-2005-4401

# Ion Velocity Measurements in a Linear Hall Thruster

Nicolas Gascon\* and Mark A. Cappelli†  
*Stanford University, Stanford, CA, 94305, USA*

and

William A. Hargus, Jr‡  
*Air Force Research Laboratory, Edwards AFB, 93524, USA*

This work presents the general operation and the near exit plane ion velocity field of the Stanford Linear Hall Thruster in a high vacuum environment. The ionized propellant velocities were measured using laser induced fluorescence of the excited state xenon ionic transition at 834.7 nm. Ion velocities were interrogated from the channel exit plane to a distance 30 mm from it. Both axial and cross-field (along the electron Hall current direction) velocities were measured. The results presented here, combined with those of previous work, highlight the high sensitivity of electron mobility inside and outside the channel, depending on the background gas density, type of wall material, or magnetic field intensity. When operated with a low background pressure, the particular Hall discharge studied here creates an ion accelerating electrostatic field mainly outside of the channel, in a narrow zone located 5-20 mm away from the exit plane.

### Nomenclature

BN	=	Boron Nitride
CVD	=	Chemical Vapor Deposition
LHT	=	Linear Hall Thruster
$B$	=	Magnetic field
$E$	=	electric field
$V$	=	ion velocity
$X$	=	transverse direction
$Y$	=	cross-field direction (along the Hall drift)
$Z$	=	axial direction (principal plume axis)

### I. Introduction

MODERN day operational Hall thrusters are closed electron-drift magnetized discharges, with uninterrupted electron Hall current<sup>1</sup>. In recent years, however, we have demonstrated the feasibility of an “open-drift”, linear Hall thruster<sup>3-5</sup>. Such geometry is attractive for scaling down the discharge, because it does not have the practical limitations imposed by the central magnet pole piece in a coaxial design. Another motivation for using a linear Hall thruster is the possibility of investigating the performance of advanced ceramic materials that are not easily machined but are available in plate form, such as chemically vapor deposited (CVD) polycrystalline diamond. This material appears to be a promising alternative to the boron nitride (BN) mixtures that are commonly used on modern Hall thrusters, due to a potential higher thermal conductivity (less mechanical stress), lower erosion rate under ion bombardment (longer lifetime), and lower secondary electron yield (higher acceleration efficiency).

\* Research Associate, Mechanical Engineering Department, MC 3032. Member, AIAA.

† Professor, Mechanical Engineering Department, MC 3032. Member, AIAA.

‡ Research Engineer, Spacecraft Propulsion Branch, 1 Ara Rd. Senior Member, AIAA.

In previous work<sup>5,6</sup>, we showed that a Hall thruster can indeed operate well with CVD diamond walls, with a lower discharge current than with BN walls (all other input parameters being equal), and with a much higher resistance to sputtering under ion bombardment (at least three times). Although we measured almost equal ion currents in the plumes of the diamond-lined and the BN-lined discharges, a hint that the former is more efficient, we did not record direct thrust and performance data at that time. Also, all those experiments were conducted in vacuum

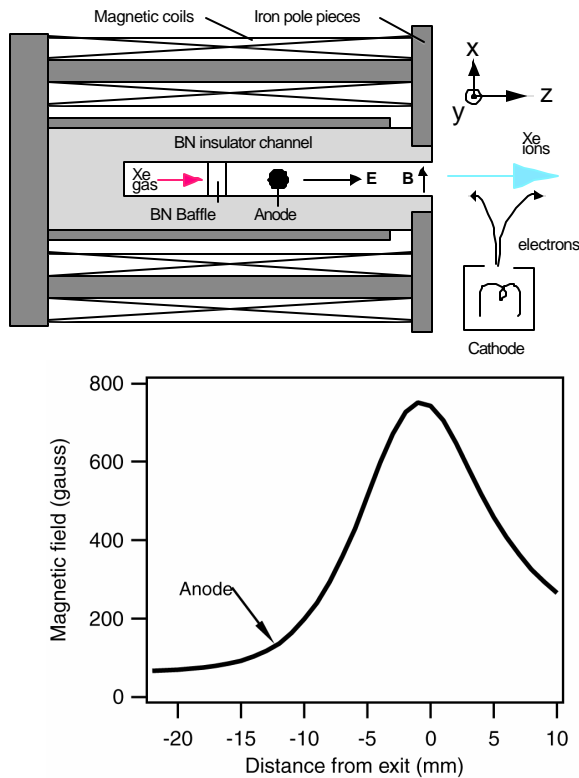


**Figure 1. Prototype Linear Hall Thruster.**  
**Top: Design details. Bottom: Magnetic field profile.**

direction follows the main  $E$  field direction, and consequently, the major axis of the ion stream.

The magnetic circuit is built from cast gray iron and consists of two rectangular solenoid coils, two front pole pieces, and one back pole piece. A magnetic screen is also used to sharpen the magnetic field profile. The circuit is capable of a peak magnetic field strength of 150 mT at 3 A of coil current; however, the coil current was kept below 1 A under vacuum to prevent melting of the kapton wire insulation. The magnetic field profile in the axial ( $Z$ ) direction for the nominal operating coil current of 1 A is shown to the bottom of in Fig. 1. The peak field for this condition is approximately 80 mT, and the field strength at the anode is over 10 mT. The field has excellent uniformity ( $<1\%$  variation) along the  $Y$  direction. The channel of this thruster is constructed to allow testing of different wall materials. The supporting channel structure is made of boron nitride, and is machined with two pockets that allow rectangular plates of different wall materials to be clamped into place. For the diamond thruster, we used 1 mm thick plates of pure CVD diamond. The surfaces facing the plasma were

chambers that had relatively high background pressures (on the order of 0.01 Pa), and we noticed that the type of pumping plant (oil diffusion or cryogenic) had a significant effect on the discharge behavior. Finally, we discovered that the diamond-lined thruster could operate in an intriguing regime, stable but pulsed, where the discharge was apparently pushed outside of the channel.

Those results prompted us to further investigate the operation and the ion dynamics of our linear Hall thruster. In the present work, we characterize the operation of the Stanford Linear Hall Thruster in the high-vacuum ( $<5.10^{-4}$  Pa) Chamber 6 facility at the Air Force Research Laboratory at Edwards AFB, and we probe the near exit ion velocity field using excited state xenon Laser Induced Fluorescence (LIF). It should be noted that the vacuum facility and experimental setup presented here were already used before to conduct an extensive study of a commercial, 200 W annular Hall thruster<sup>7</sup>.

## II. Experiments

### A. Thruster

The details of the linear Hall thruster operated here are described in previous papers<sup>5,6</sup>. The discharge and the experimental set-up, along with the coordinate system used in this paper, are shown to the top of Fig. 1. Note that the  $X$  direction corresponds to the radial direction in a classical (annular) Hall thruster. The  $Y$  direction is parallel to the  $E \times B$  electron drift. The  $Z$

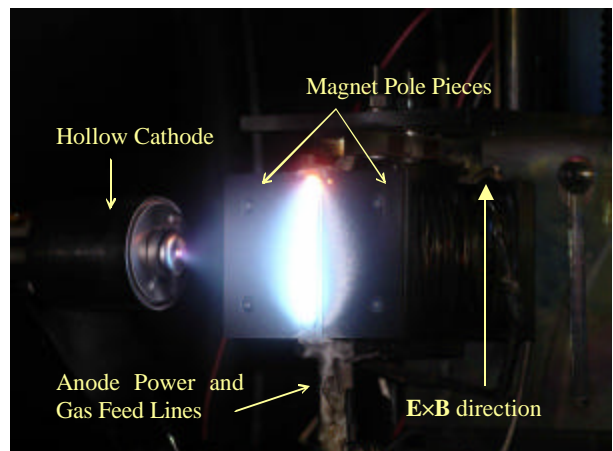


**Figure 2. Stanford LHT viewed from a 45° angle, operating in AFRL chamber 6.**

polished to a mirror finish. For the comparison case, we used boron nitride plates of the same geometry as the diamond plates.

A boron-nitride baffle separates a plenum from the anode, a tungsten rod 1.6 mm in diameter. A commercial hollow cathode (Veeco/IonTech HCN-252) is used to neutralize the ion beam. The cathode is located 30 mm downstream of the channel exit, 45 mm from the channel in  $X$  and centered in  $Y$ . The thruster is mounted such that the  $Y$  direction is vertical and the  $X$  and  $Z$  directions are horizontal. The anode power and gas feed lines come from the bottom (see Fig. 2). The electromagnet current polarity is chosen such that the Hall electron current due to  $E_z \times B_x$  drift is up in the laboratory frame. During thruster operation, the discharge chamber wall facing this current turns red hot due to the intense electron bombardment, as can be clearly seen in Fig. 2.

The nominal input parameters are: anode xenon flow rate, 0.6 mg/s; electromagnet current, 1A; discharge voltage, 200 V; cathode xenon flow rate, 0.15 mg/s. Both the BN-channel and diamond-channel thrusters proved capable of continuous operation at voltages as high as 300 V.

### B. Vacuum facility and diagnostics

The measurements presented in this work were performed in Chamber 6 at the Air Force Research Laboratory's (AFRL) Electric Propulsion Laboratory at Edwards Air Force Base in California. The vacuum facility is a nonmagnetic stainless steel chamber which has a 1.8 m diameter and 3.0 m length. It has a measured pumping speed of 32,000 l/s on xenon. Pumping is provided by four single stage cryo-panels (APD single stage cold heads at  $\sim 25$  K) and one 50 cm two stage APD cryo-pump ( $< 12$  K). Chamber pressure during thruster operation is approximately  $5 \times 10^{-4}$  Pa, corrected for xenon. During thruster operation, the macroscopic parameters (discharge voltage, anode current, etc.) are monitored and recorded at a 1Hz data rate with an Agilent data logging system. Figure 3 shows a side-view diagram of the Hall thruster inside AFRL Chamber 6. The thruster is mounted on a three axis orthogonal computer controlled translation system.

Figure 3 also shows the two orthogonal LIF probe beams and windows through which the beams enter the chamber. Figure 4 shows a top view of the laser optical train, collection optics, and one leg of the external probe optics. The laser used is a New Focus Vortex tunable diode laser. It is capable of tuning approximate  $\pm 50$  GHz about a center wavelength of 834.7 nm. The 10 mW beam is passed through a Faraday rotator to eliminate feedback to the laser. The laser beam then passes through several beam pick-offs until it reaches a 50-50 beam splitter (BS /) where it is split into two beams of equal power. The first beam, the axial probe beam shown in Figs. 3 and 4, is focused by a lens and enters the vacuum chamber through a window. A second probe beam, shown in Fig. 3 only, is directed from the optical bench

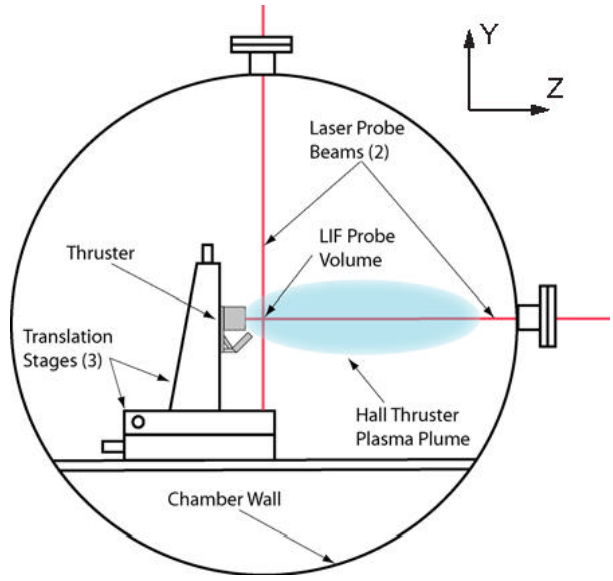


**Figure 3. Side view diagram of thruster within AFRL chamber 6. Also shown are the translation stages and the laser probe beams**

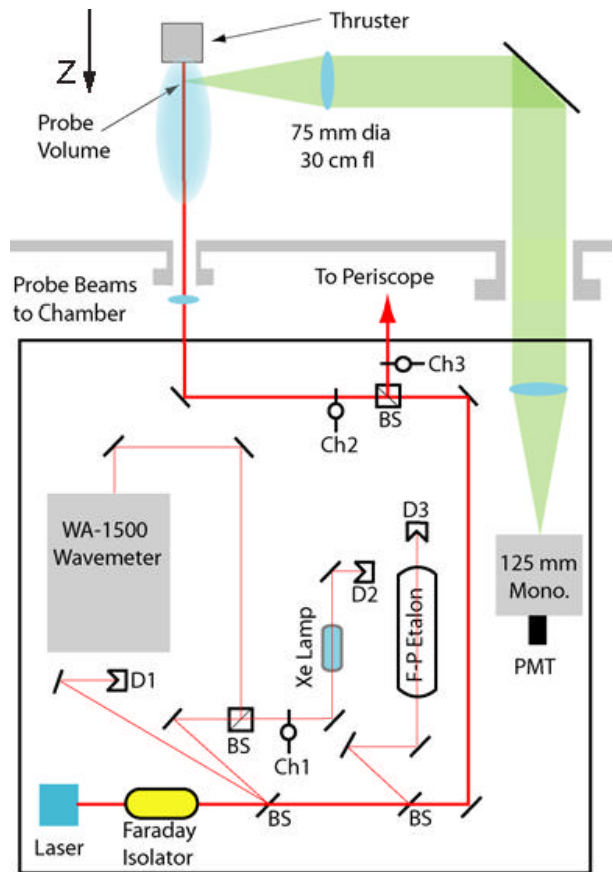


**Figure 4. Top view diagram of the laser optical train and collection optics.**

via a periscope apparatus so that it enters the chamber from above the thruster and probes the velocity perpendicular to the first probe beam. Each probe beam is chopped at a unique frequency by choppers Ch2 (2 kHz) and Ch3 (2.8 kHz) for phase sensitive detection of the fluorescence signals.

The two wedge beam pick-offs (BS /) shown in Fig. 4 provide portions of the beam for diagnostic purposes. The first beam pick-off directs a beam to a photo diode detector (D1) used to provide constant power feedback to the laser. The second beam is divided into two equal components by a 50-50 beam splitter. The first component is directed to a Burleigh WA-1500 wavemeter used to monitor absolute wavelength. The second component is sent through chopper Ch1 (1.3 kHz) and through a low pressure xenon hollow cathode discharge lamp. The lamp provides a stationary absorption reference for the determination of the Doppler shift. Unfortunately, there is no detectable population of the ionic xenon state. However, there is a nearby (18.2 GHz distant) neutral xenon transition at 834.68 nm. Absorption of this neutral xenon transition provides a stationary reference for measurement

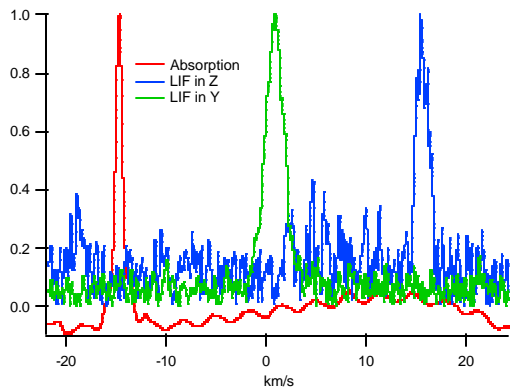


**Figure 5. Sample LIF/absorption traces. All signals have been normalized. BN walls, nominal operating conditions,  $z = +30$  mm,  $x = y = 0$ .**

of the Doppler shifted ionic transition. The second pick-off sends a beam to a 300 MHz free spectral range Fabry-Perot etalon (F-P). This instrument provides high resolution frequency monitoring of the wavelength interval swept during a laser scan. The fluorescence collection optics are also shown in Fig. 4. The fluorescence is collected by a 75 mm diameter, 300 mm focal length lens within the chamber. The collimated signal is directed through a window in the chamber side wall to a similar lens that focuses the collected fluorescence onto the entrance slit of 125 mm focal length monochromator with a Hamamatsu R928 photomultiplier tube (PMT) detector. Due to the 1:1 magnification of the collection optics, the spatial resolution of the measurements is determined by the geometry of the entrance slit 1 mm width and 1.7 mm height.

The laser is controlled by an analog ramp signal generated by a National Instruments E-series data acquisition board. During each laser scan, the data acquisition card records the absorption and two fluorescence signals using three lock-in amplifiers. The signal from the Fabry Perot etalon photodiode detector (D3) signal is amplified and filtered using a current preamplifier. The output of which is also recorded. Typically, the scans span 55 GHz. Each scan yields four traces of several thousand points. The traces are then stored for post processing.

The origin of all the velocity maps is located at the thruster exit plane, centered in the  $Y$  and  $X$  direction. For the experiments presented here, the thruster was moved along the  $Z$  direction (i.e. along the principal direction of the plasma), as far as 30 mm away from the exit plane. The LIF apparatus allowed measuring the ion velocity components along the  $Z$  and  $Y$  axis. Figure 5 shows an example of processed scan, with the  $V_Z$  and  $V_Y$  distributions, and the reference absorption signal. For this particular scan, the velocity distributions are close to gaussians with half-widths on the order of a few km/s. The  $V_Z$  distribution peaks near 16 km/s, corresponding to an ion energy of about 170 eV (as a reminder, the discharge voltage is 200 V). The  $V_Y$  distribution peaks near 2 km/s in the positive ( $E_z \times B_y$ ) direction, which results probably from the asymmetry caused by the electron Hall current. In other scans not shown here, the velocity distributions came out less regular the ones in Fig. 5, which can be explained by several mechanisms: an ionization zone widely spread across the plasma potential drop, bulk plasma oscillations<sup>8</sup>, or momentum and charge exchange collisions with the xenon atoms. In the LIF maps presented below, we chose to plot the most probable velocity component (peak of the velocity distribution) together with the average velocity component (i.e. the first moment of the distribution).

The origin of all the velocity maps is located at the thruster exit plane, centered in the  $Y$  and  $X$  direction. For the experiments presented here, the thruster was moved along the  $Z$  direction (i.e. along the principal direction of the plasma), as far as 30 mm away from the exit plane. The LIF apparatus allowed measuring the ion velocity components along the  $Z$  and  $Y$  axis. Figure 5 shows an example of processed scan, with the  $V_Z$  and  $V_Y$  distributions, and the reference absorption signal. For this particular scan, the velocity distributions are close to gaussians with half-widths on the order of a few km/s. The  $V_Z$  distribution peaks near 16 km/s, corresponding to an ion energy of about 170 eV (as a reminder, the discharge voltage is 200 V). The  $V_Y$  distribution peaks near 2 km/s in the positive ( $E_z \times B_y$ ) direction, which results probably from the asymmetry caused by the electron Hall current. In other scans not shown here, the velocity distributions came out less regular the ones in Fig. 5, which can be explained by several mechanisms: an ionization zone widely spread across the plasma potential drop, bulk plasma oscillations<sup>8</sup>, or momentum and charge exchange collisions with the xenon atoms. In the LIF maps presented below, we chose to plot the most probable velocity component (peak of the velocity distribution) together with the average velocity component (i.e. the first moment of the distribution).

### III. Results and discussion

Figure 5 shows the current voltage characteristics of the Stanford LHT for various combinations of wall materials (BN or diamond), anode xenon flow rate (0.9 or 0.6 mg/s) and electromagnet current (0.5 or 1.0 A). It is apparent from these curves that the LHT discharge current does not reach a plateau at high applied voltages (>150 V) but continues to increase, unlike what is observed with most modern, co-axial Hall thrusters. This seems to indicate that in the case of the LHT, a voltage-dependent mechanisms provides an added electron current in the discharge when the ionization fraction has reached a maximum. We surmise that this additional current is a cross field electron flow created by a strong near-wall conductivity effect<sup>9</sup> on the channel side facing the Hall current.

The nature of the wall material, boron nitride or CVD diamond, does not seem to have a significant impact on the discharge current. However, our previous studies of this particular linear Hall discharge using diamond instead of boron nitride for the channel inserts always resulted in a lower discharge current, or even a change in operating regime<sup>5,6</sup>. Figures 7 and 8 further reveal that when the LHT is operated in AFRL Chamber 6, the ion dynamics in the plume is mostly unaffected by the type of channel wall inserts, and that the major part of ion acceleration occurs outside the thruster, 5-20 mm away from the exit plane. We may relate those surprising results to the background pressure in the test facility: when the neutral gas density is high outside of the thruster, as in Refs. 26, collisions between atoms and electrons account for a high cross-magnetic field mobility, and most of the plasma potential drop occurs inside the channel. In the experiments presented here, the results suggest that the cross-field electron mobility due to the background gas *outside* the channel is lower than the one due to the side wall *inside* the channel.

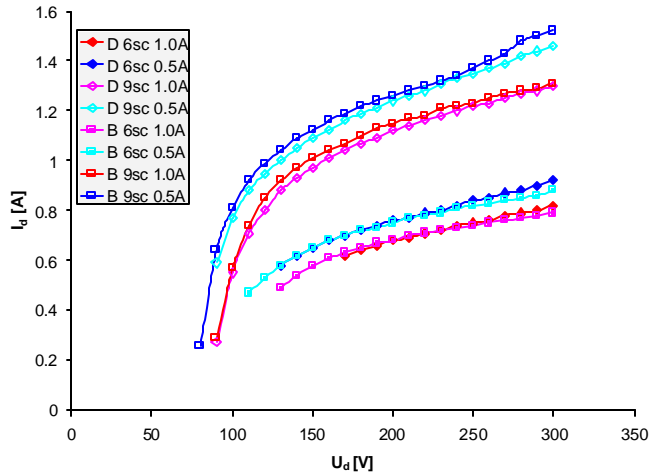


**Figure 6. Current-Voltage characteristics of the Stanford LHT for various operating conditions. Squares: with BN walls. Diamonds: with CVD diamond walls. Full Markers: 0.6 mg/s anode flow rate. Empty Markers: 0.9 mg/s anode flow rate. Blue Plots: 0.5 A electromagnet current. Red Plots: 1.0 A electromagnet current.**

The effect of background neutral gas is again illustrated in Fig. 9, where the cathode xenon flow rate is doubled compared to the nominal condition. In this case, there is almost no ion acceleration around the location of the cathode ( $z = 30$  mm), indicating a weak electrostatic field and a high electron cross-magnetic field mobility.

One can also notice in Fig. 9 a greater difference between the most probable velocities and the average velocities than in Fig. 7. This is probably a result of the ion velocity distribution being affected by the low energy ion population created by charge exchange collisions near the cathode.

Finally, the experimental series presented in Figs. 11 and 12 aims at assessing the effect of the magnetic field on the acceleration zone. As expected, when the magnetic flux density is divided by two, the acceleration is less sharp and occurs further away from the channel exit plane, which illustrates the direct effect that the magnetic field has on the electron mobility in the discharge.

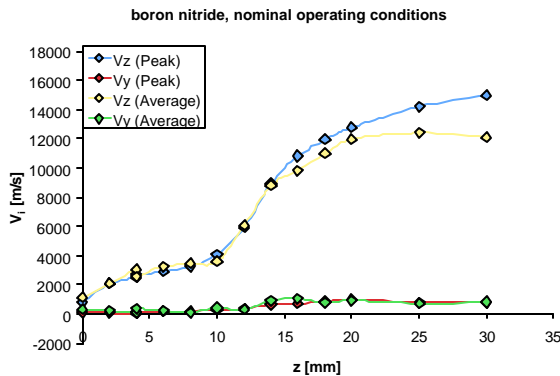


**Figure 7. Velocities for BN walls, nominal case.**

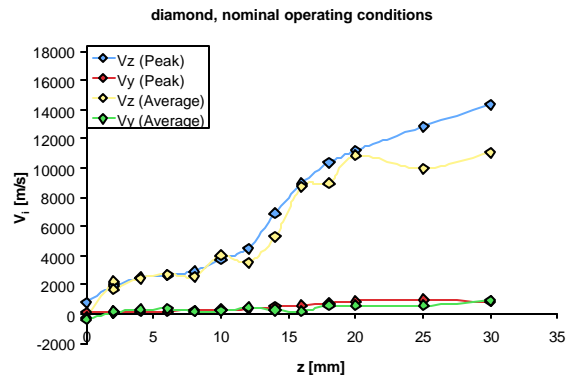


**Figure 8. Velocities for diamond wall, nominal case.**

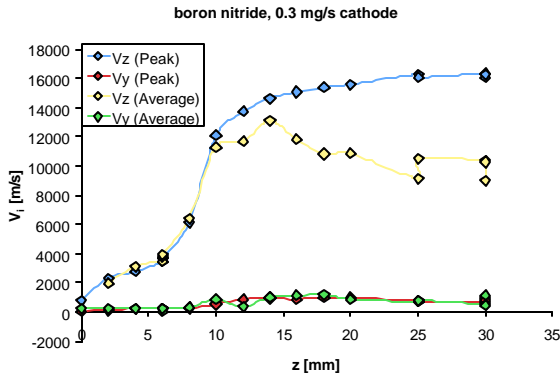


Figure 9. Velocities for BN walls LHT with increased cathode flow.

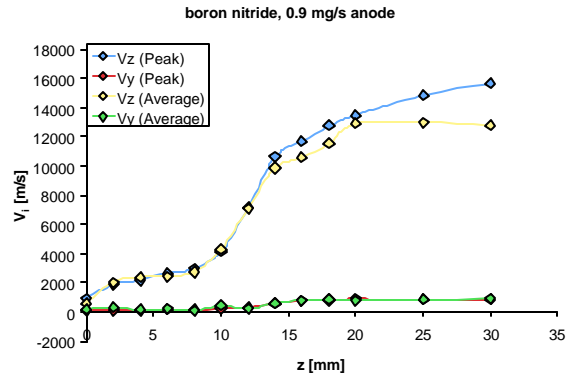


Figure 10. Velocities for BN walls LHT with increased anode flows.

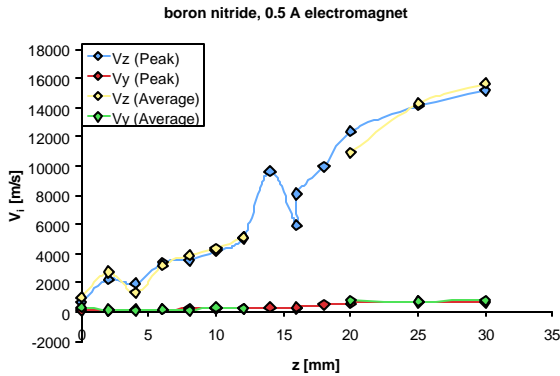


Figure 11. Velocities for BN walls LHT with reduced magnetic field.

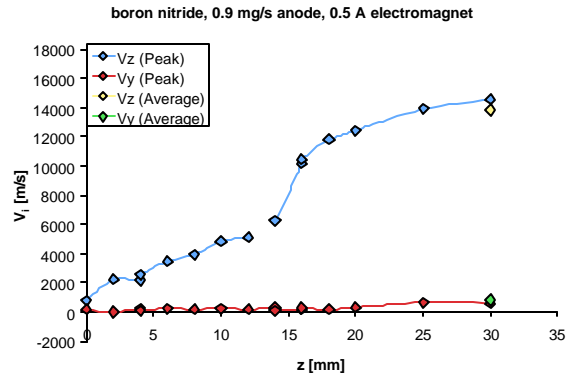


Figure 12. Velocities for BN walls LHT with increased anode flow and reduced magnetic field.

#### IV. Summary and Future Work

We have parametrically investigated the operation of a Linear Hall thruster in a high vacuum environment, and conducted a Laser Induced Fluorescence mapping of the near exit xenon ion velocity field. These results, combined with those of previous work, highlight the high sensitivity of electron mobility inside and outside the channel, depending on the background gas density, type of wall material, or magnetic field intensity. When operated with a low background pressure, the particular Hall discharge studied here creates an ion accelerating electrostatic field mainly outside of the channel. Such a configuration may be attractive from an engineering perspective, with the prospect of reducing thruster wear due to high-energy ion bombardment. Further studies will include direct thrust measurements to assess the efficiency of the plasma acceleration.

#### Acknowledgments

This work is funded in part by the Air Force Office of Scientific Research. The authors would like to thank J. Zimmer and J. Herlinger at  $sp^3$  Inc. (Mountain View, California) for providing the diamond plates used in this study.

#### References

- <sup>1</sup>Zhurin V. V., and Kaufman H. R., "Physics of Closed Drift Thrusters" *Plasma Sources Sci. Technology* **8**, pp. R1-R20, 1999.
- <sup>2</sup>Hargus W. A., Jr, and Cappelli M. A., "Development of a Linear Hall Thruster", *34<sup>th</sup> Joint Propulsion Conference, Cleveland, OH*. American Institute of Aeronautics and Astronautics, Washington, DC, 1998. AIAA-98-3336.

<sup>3</sup>Schmidt D. P., Meezan N.B., Hargus W.A., Jr., and Cappelli M.A., “A Low-Power, Linear-Geometry Hall Plasma Source with an Open Electron-Drift,” *Plasma Sources Science and Technology* 9, pp. 68-76, 2000.

<sup>4</sup>Cappelli M.A., Walker Q.E., Meezan N.B., and Hargus W.A., Jr., “Performance of a Linear Hall Discharge with an Open Electron Drift”, *37<sup>th</sup> Joint Propulsion Conference, Salt Lake City, UT*, American Institute of Aeronautics and Astronautics, 2001. AIAA-2001-3503.

<sup>5</sup>Meezan N. B., Gascon N., and Cappelli M. A., “Linear Geometry Hall Thruster with Boron Nitride and Diamond Walls”, *27<sup>th</sup> International Electric Propulsion Conference, Pasadena, CA*. Electric Rocket Propulsion Society, 2001. IEPC-01-39.

<sup>6</sup>Gascon, N., Thomas, W. A., Hermann, W. A., and Cappelli M. A., “Operating regimes of a linear SPT with low secondary electron-induced wall conductivity”, *39<sup>th</sup> AIAA/ASEE/ASME Joint Propulsion Conference, Huntsville, Alabama*. American Institute of Aeronautics and Astronautics, Washington, DC, 2003. AIAA-2003-5156.

<sup>7</sup>Hargus W. A., Jr, and Charles C., “Near Exit Plane Velocity Field of a 200 W Hall Thruster”, *39<sup>th</sup> AIAA/ASEE/ASME Joint Propulsion Conference, Huntsville, Alabama*. American Institute of Aeronautics and Astronautics, Washington, DC, 2003. AIAA-2003-5154

<sup>8</sup>Bareilles J., Hagelaar G. J. M., Garrigues L., Boniface C., Boeuf J. P. and Gascon N., “Critical Assessment of a Two-Dimensional Hybrid Hall Thruster Model: Comparisons with Experiments”, *Physics of Plasmas* Vol. 11, No 6, pp. 3035-3046, 2004.

<sup>9</sup>Barral, S., Makowski, K., Peradzynski, Z., Gascon, N., and Dudeck, M., “Wall Material Effects in Stationary Plasma Thrusters II: Near-Wall and Inner-Wall Conductivity,” *Physics of Plasmas*, Vol. 10, No. 10, Oct. 2003, p. 4137.